Influence of Strontium phosphate Coating on the Degradation of Physical Vapor Deposition Sprayed Mg Coating on Ti6Al4V Substrate to Promote Bone Tissue Healing

Muhammad Ibrahim[1,2], Xiaoming Yu[3], Lili Tan[1]* and Ke Yang[1]*

[1] Institute of Metal Research, Chinese Academy of Science, Shenyang, China, [2] School of Materials Science and Engineering, University of Science and Technology of China, Shenyang, China, [3] School of Material Science and Engineering, Shenyang Ligong University, Shenyang, China

Ti6Al4V is one of the commonly used orthopedic metallic materials, but its bioactivity is weak, which makes it challenging to produce bone integration between material and bone tissue. In this study, an Mg/SrP composite coating was prepared on Ti6Al4V, to promote bone tissue healing and shorten the healing cycle. The surface characterization, *in vitro* degradation performance and bioactivity of the composite coating, were investigated. The results revealed that Mg/SrP composite coating has more suitable degradation rate than Pure Mg, no cytotoxicity was found on the Mg/SrP composite coated samples, higher proliferation compared with the culture medium was found, indicating that the Mg/SrP composite coating is a candidate coating on Ti6Al4V to improve the bioactivity.

Keywords: Ti alloy, Mg/SrP coating, degradation, biocompatibility, Mg coating

INTRODUCTION

Ti-based metal is one of the metallic materials used in dentistry and orthopedic surgery to enhance or support or to replace an existing biological structure (Zhang and Chen, 2019; Hafeez et al., 2020; Liu et al., 2020). Most of these medical devices are made of pure Ti and its alloy, because of their excellent biocompatibility, enhanced corrosion resistance, and unique mechanical properties (Liu et al., 2004; Gode et al., 2015; Yu et al., 2018b; Ebrahimi et al., 2019; Ibrahim et al., 2020). In the 1950s, Per-Ingvar Branemark discovered the principles of osteointegration for the first time (Le et al., 2014). However, Ti-based metal has still some shortcomings yet to be resolved. The major challenge for Ti is to improve the osteointegration and enhance the bioactivity of the implants for bone regeneration and healing (Drago and Howell, 2012; Attarilar et al., 2019; Wang et al., 2020). 3D printed porous structure and surface modification are the conventional approaches to improve bone growth and enhance the bioactivity of Ti. Surface modifications such as CaP coating could accelerate bone growth, and the physicochemical changes of the implant could induce a firm bonding with the bone (Li et al., 2017).

Recently, Mg-based metals have shown great potential to be used as biocompatible and biodegradable materials, because of their excellent properties, including relatively close elastic modulus and density (41–45 GPa, 1.7–2.0 g/cm^3) to the human bones (10–40 GPa, 1.8–2.1 g/cm^3) (Staiger et al., 2006; Witte et al., 2006; Kraus et al., 2012; Sun et al., 2012; Yu et al., 2018a). Mg also exhibits a positive effect on bone tissue, which could improve the reconstruction and healing of the associated bone. Witte (2015) reported that Mg-based metals
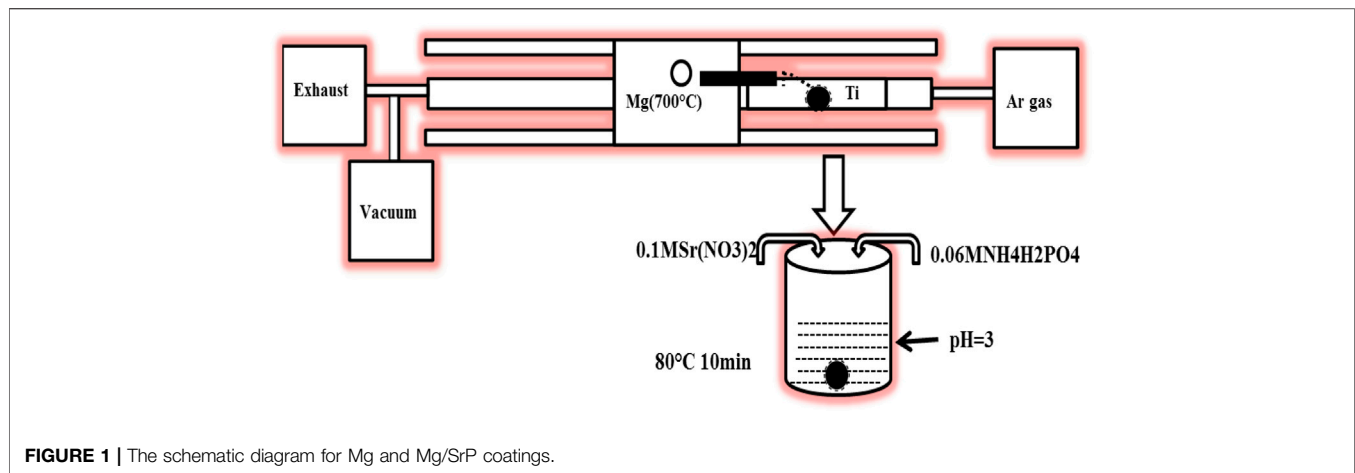
FIGURE 1 | The schematic diagram for Mg and Mg/SrP coatings.

showed a positive impact on the bone tissue, and high Mg ions activated the surrounding bone cells (Wang et al., 2015). Zhai et al. (2014) found that Mg also has a strong effect on the apoptosis of osteoclasts and osteoblast, and influences the proliferation. Therefore, Mg coating on Ti can enhance its osteointegration properties. The main problem that exists for Mg coating is its fast degradation (Salunke et al., 2011), mainly when applied on implants with large surface area exposed to the body fluid, leading to large pieces of layer peeling off the substrate and the high alkaline environment around the implants limits its application as a bone implant coating.

Strontium phosphate (SrP) a biocompatible coating was used to control the degradation rate of pure Mg. Sr^{2+} ions have the function to reduce bone resorption and cause to promote bone regeneration (Boyd et al., 2015). Further SrP coating has excellent corrosion rate and has been developed explicitly for biocompatible orthopedic implants (Ke et al., 2014). The morphology, size, concentration, charge, and surface properties; all of them have a high impact on preventing toxicity and harmful effects (Attarilar et al., 2020). To improve the biological function of Ti6Al4V alloys, some nanoscale (Mg, Sr)-HA powders were coated on its surface (Cao et al., 2019).

Therefore, in this work, a Mg/SrP composite coating was deposited on the surface of the Ti alloy, to regulate the degradation behavior of Mg-based metal coating, further promote the bone tissue healing and shorten the healing cycle of Ti alloy with the Mg^{2+} ions release from the surface. The biocompatibility and corrosion resistance of Mg/SrP composite coating on Ti alloy was also studied.

EXPERIMENTAL DETAILS

Materials and Methods

The schematic diagram of the Mg and Mg/SrP coatings preparation process is shown in **Figure 1**. Mg coatings were deposited on Ti6Al4V samples with a dimension of Φ 10 mm × 3 mm by Physical Vapor Deposition (PVD) method. Firstly Ti6Al4V substrate was polished, washed, ultrasonically cleaned, and then dried. The vapor generated from the source

of pure Mg (99.99 wt%) at 700°C was carried by an Ar flow of 250 sccm and deposited on the substrate at a temperature of 300°C. The vacuum pumps allowed the pressure of 10^{-1} Torr to collect the high purity Mg. In the designing or optimization of PVD, the coating thickness varies with the variation of source and substrate distance. So it is essential to control the gap between the source and substrate to control its depth because the coating with higher thickness lowered the coating adhesion and possibly may affect the bone tissue healing.

Mg coated samples were then treated with SrP coating. The SrP coating solution consisted of 0.06 M $NH_4H_2PO_4$ and 0.1 MSr $(NO_3)_2$. The dilute HNO_3 was used to adjust the pH to 3, and then the samples were immersed in the solution for 10 min at 80°C. The coated samples were washed with ethanol and then warmly dried.

Characterization of Coatings

The surface and cross-section morphology of Mg and Mg/SrP coatings were observed by scanning electron microscope (SEM, S-3400 N) equipped with a dispersive energy spectrum (EDS). Furthermore, the compositions of the layers were characterized by X-ray diffractometry (XRD, Bruker D8 ADVANCE) using the CuKα line generated at 40 kV and 35 mA.

Electrochemical Test

A Gamry instrument (Reference 600) was used to examine the electrochemical corrosion test. The samples used for this purpose had an exposed area of 0.785 cm^2 and were molded in the epoxy resin. D-Hank's was used to perform the test at a temperature of 37°C. The composition of D-Hank's solution was listed in Table 1. The three-electrode cell used for this purpose consists of platinum as the counter electrode; a saturated calomel electrode as a reference electrode and the coated samples were working electrode. After the 1800 s, the test started at an open-circuit potential (OCP). At a frequency range of 100 kHz to 10 MHz, the electrochemical impedance spectroscopy (EIS) was carried out at the OCP. Concerning OCP, the potentiodynamic polarization test started at a scan rate of 0.5 mV/s and a voltage of −0.25 to 0.35 V. For each coated sample the experiment was repeated three
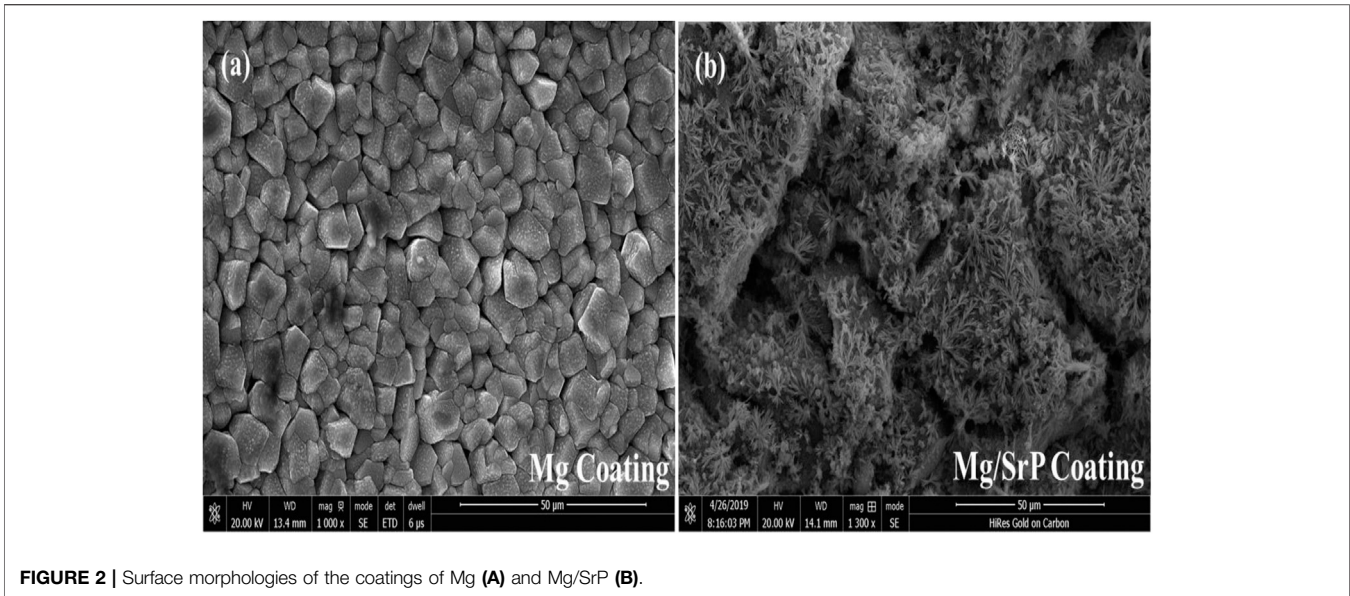
FIGURE 2 | Surface morphologies of the coatings of Mg **(A)** and Mg/SrP **(B)**.

times. The corrosion rate of Mg and Mg/SrP coating was measured with the following equation (Chen et al., 2019). I_{corr} the corrosion current density of the coating is measured by Tafel extrapolation of polarization curve, I_{corr} is related to P_i (average corrosion rate) in mm/year using the equation.

$$P_i = 22.85_{Icorr} \qquad (1)$$

Immersion Test and Mg²⁺ Release

Mg and Mg/SrP coated samples with a size of $\Phi 10$ mm $\times$ 3 mm were immersed in D-Hank's solution for nine days at the ratio of 1.25 cm²/ml. The immersion solution was changed after each 24 h to keep it fresh. The pH value was recorded every 24 h before refreshing the solution. The release of Mg²⁺ from each sample in

FIGURE 3 | XRD pattern of Mg and Mg/SrP coatings on Ti alloy.

D-Hank's solution at 1, 2, 3, 4, 5, 6, and 7 days were determined by using inductive-coupled plasma mass spectrometry (ICP-MS, Thermo, United States).

Cell Proliferation

MC3T3-E1 mouse preosteoblast cells were purchased from the College of Stomatology, Fourth Military Medical University, Xi'an, China. The α-MEM complete medium supplemented with 10% heat-inactivated fetal bovine serum, 100 U/ml penicillin, and 100 mg/ml streptomycin, were used for cell culture under the condition of 5% CO_2 at 37°C. MC3T3-E1 incubated cells were seeded on Mg and Mg/SrP coated samples in a 96-well plate with an initial density of 4×10^4 cells. Kit-8 (CCK-8, Japan) was used for this purpose. The cultured medium at the time point of 1, 3, and 5 days was transferred to new 96-well culture plates. CCK-8 solution (10% volume) was added onto the plates and incubated for 3 h at 37°C. A microplate reader was then used to quantify the absorbance of the solutions at 450 nm wavelength with a plate reader.

Statistical Analysis

Data were expressed in standard deviation (SD) and statistically, one-way analysis of variance (ANOVA) was analyzed with a post-hoc Tukey test. The significant P values of less than 0.05 were considered.

RESULTS AND DISCUSSION

Characterization of Coatings

Figure 2 presents the surface morphology of Mg and Mg/SrP coatings on the Ti substrate. Mg coating deposited smoothly and densely with an average particle size of 7 μm (**Figure 2A**). From the Mg/SrP composite coating observation, a small crystal-like
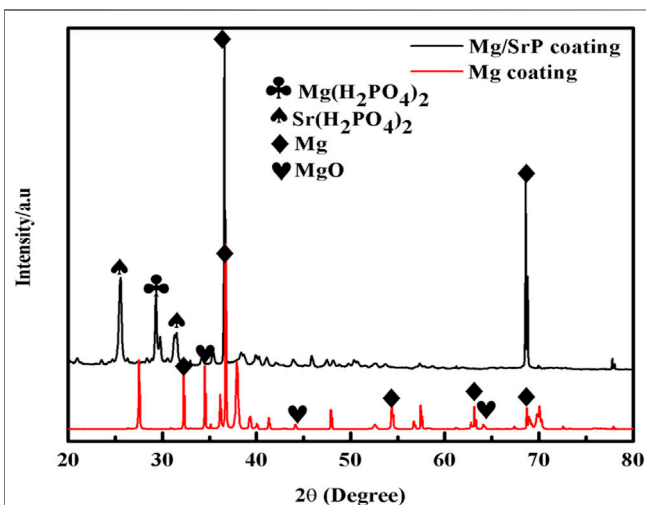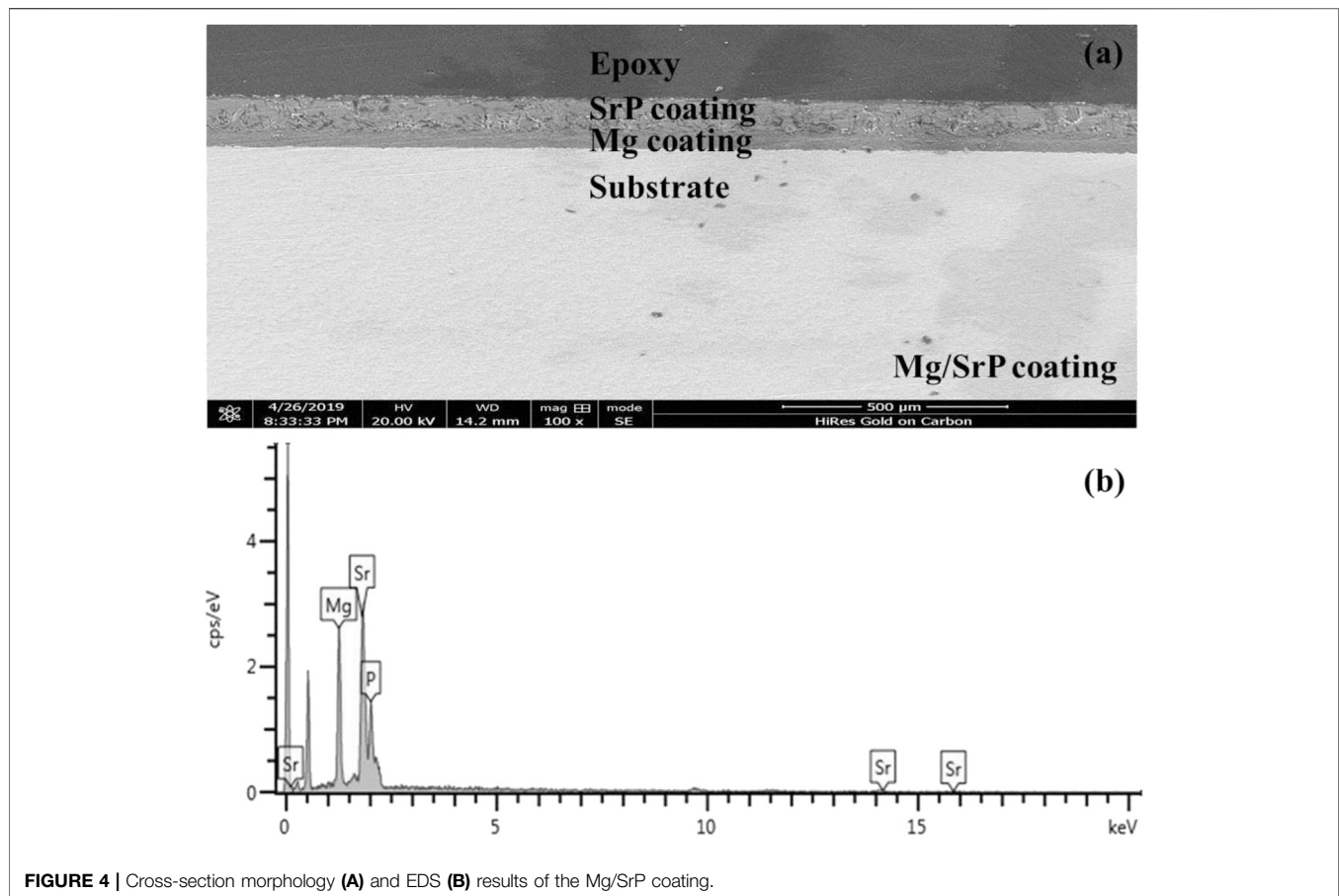
FIGURE 4 | Cross-section morphology **(A)** and EDS **(B)** results of the Mg/SrP coating.

pattern was observed (**Figure 2B**). From EDS analysis, there are Mg, Sr, and P elements in the Mg/SrP coating. Further analysis of the coating layer was carried out from the XRD pattern (**Figure 3**). The Mg coating consists of both Mg and MgO. In the Mg/SrP coating, in addition to the diffraction peak of the Mg, the existence of diffraction peaks belonging to $Sr(H_2PO_4)_2$ and $Mg(H_2PO_4)_2$ indicates the presence of crystallization in the coating, which arguments the strength of the coating with substrate because the coating strength with the substrate is a key factor for evaluation of its performance. Also, the low adhesion strength possibly delaminates the coating layer from the surface, which may cause the failure of the implant. Previous studies also reported the importance of coating strength with the substrate (Cao et al., 2019).
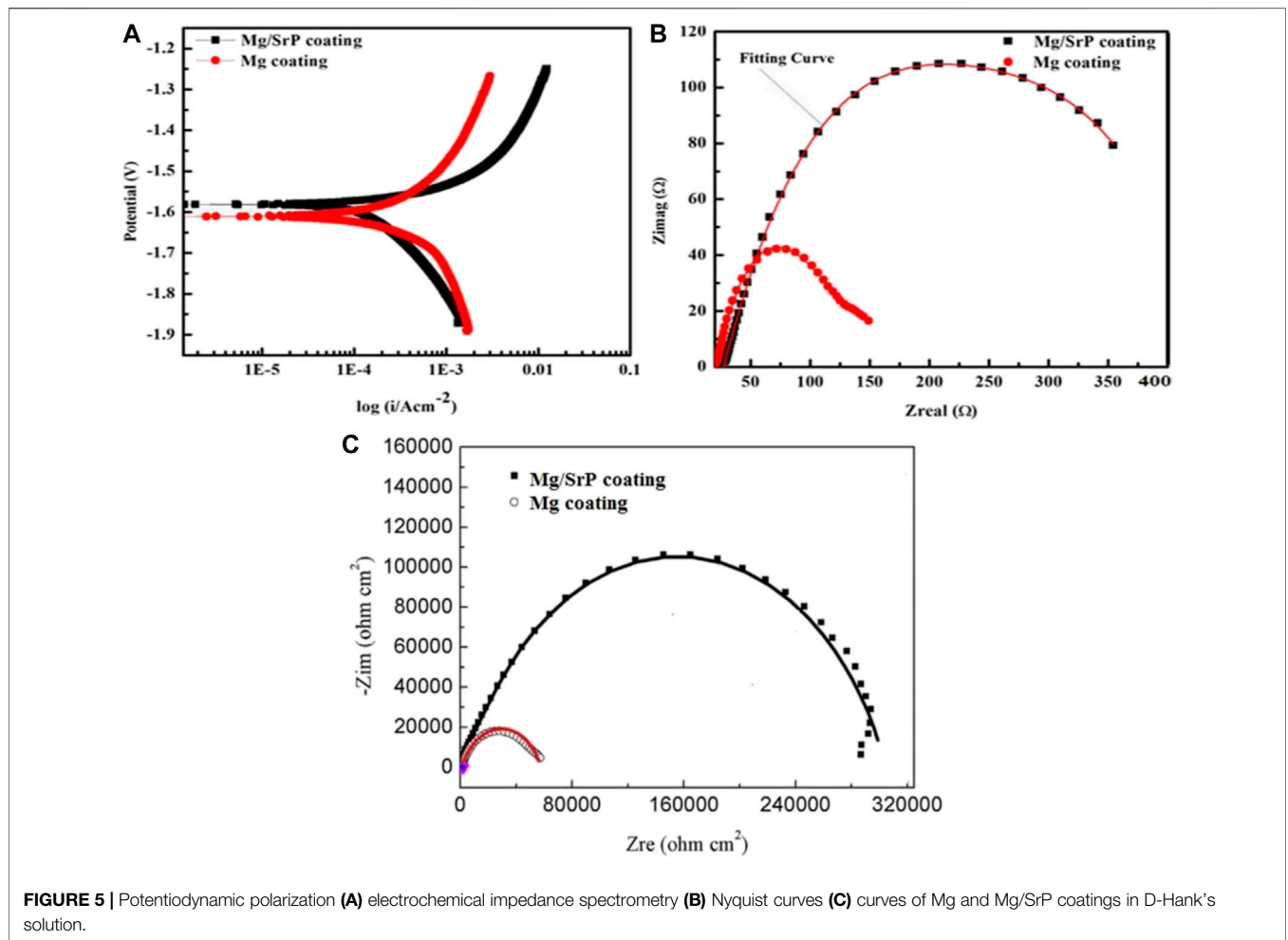
From the cross-section morphology of the coating shown in **Figure 4**, it can be seen that the thickness of Mg coating was about 50–52 μm and that of Mg/SrP was 99–101 μm (**Figure 4A**).

Electrochemical Measurements

The electrochemical corrosions of Mg and Mg/SrP coatings were characterized by potentiodynamic polarization curves and electrochemical impedance spectrometry. **Figure 5** showed the polarization curves and impedance spectra in D-Hank's solution at 37°C for both Mg and Mg/SrP coatings. **Table 2** presents the Tafel fitting results of both kinds of coating

surfaces. From the results we can see that the Mg/SrP coating exhibited a lower current density of 0.700 ± 0.02 μA/cm^2 compared to that of Mg coating (3.400 ± 1.01 μA/cm^2), the corrosion rate of Mg/SrP coating is approximately 0.103 ± 0.01 mm/year, also less than that of Mg (0.52 ± 0.21 mm/year). Similarly, from electrochemical impedance spectrometry (EIS), the higher the arc in the impedance spectrometry is, the higher the corrosion resistance of the material is. Hence, the corrosion resistance of the Mg/SrP coating is significantly higher than that of Mg coating (**Figure 5B**), which is also consistent with the potentiodynamic polarization curve. It implies that the SrP coating shows more resistant to corrosion than the Mg coating.

Figure 6 shows the equivalent circuit of Mg and Mg/SrP coating and **Table 3** shows the fitted data obtained with ZSimp Win software. C is the double-layer capacitance of solution and coating surface, Y04 is the constant phase element, whereas R_1 and R_2 show the solution and charge transfer resistance, respectively. From **Table 3** R_2 shows better corrosion resistance. The corrosion resistance of coating increases with SrP. To analyze the degradation of coating impedance is usually adopted. From impedance curves in **Figure 5**, one capacitive loop can be found on the Nyquist plot of the coating with Mg and Mg/SrP coating. Usually, a larger diameter of the circuit and higher impedance means better corrosion resistance of the

FIGURE 5 | Potentiodynamic polarization **(A)** electrochemical impedance spectrometry **(B)** Nyquist curves **(C)** curves of Mg and Mg/SrP coatings in D-Hank's solution.

coating **Table 3**. Therefore Mg/SrP coating exhibited the highest degradation resistance.

Immersion Test

Biodegradable materials are implant materials gradually corroded *in vivo*, with the release of corrosion products, which dissolve completely and assist the healing tissue without implant residues (Li et al., 2014a). Biodegradable Mg-based materials have been investigated widely, due to its unique degradation in the physiological environment, to avoid the repeated surgery of

implants (Staiger et al., 2006; Chai et al., 2012; Zheng et al., 2014). Mg having similar mechanical properties with human bones and have a positive effect on the growth of bone tissue (Witte et al., 2008). The pH and Mg^{2+} ion release results of the coated samples immersed in D-Hank's solution shown in **Figure 7**. The products arising from the degradation of Mg influence apoptosis of osteoclasts and proliferation of osteoblasts has been observed to activate bone cell (Witte et al., 2005; Li et al., 2014b).
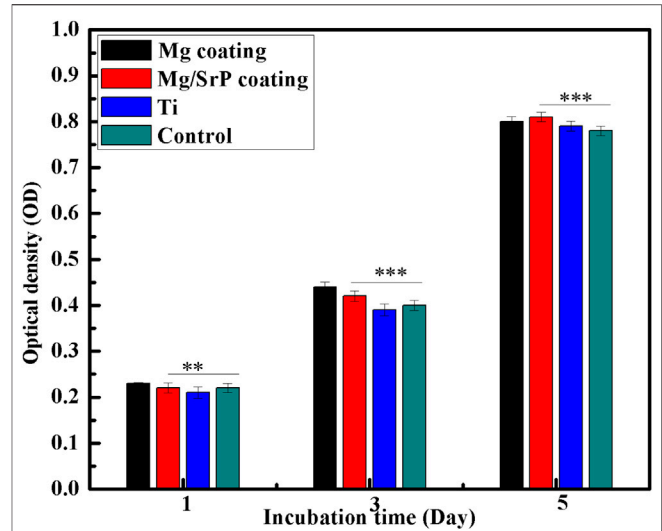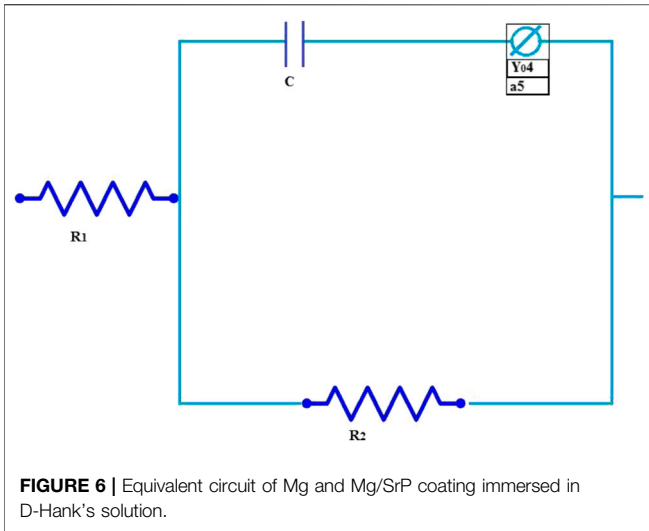
From the variation of pH, it can be seen that the pH value of Mg coated sample rises rapidly on the first day of immersion in D-Hank's solution to around 11, reaching a maximum, and this is significantly higher than the Mg/SrP coated sample and the blank control sample. In the following days, the pH value is on a downward trend, and the overall pH value drops rapidly. The pH of the Mg/SrP coated sample shifts up quickly to 9.75 after

TABLE 1 | The composition of D-Hank's solution (g/L).

KCl	KH_2PO_4	NaCl	$Na_2HPO_4.7H_2O$	$NaHCO_3$	$C_{19}H14O_5S$
0.4	0.06	8	0.06	0.35	0.02

TABLE 2 | Tafel fitting results based on potentiodynamic polarizations tested in D-Hank's solution.

Samples	Potential (V)	Current density ($\mu A/cm^2$)	Corrosion rate (mm/year)
Mg coating	−1.620 ± 0.02	3.400 ± 1.01	0.521 ± 0.21
Mg/SrP coating	−1.580 ± 0.01	0.700 ± 0.02	0.103 ± 0.01

FIGURE 6 | Equivalent circuit of Mg and Mg/SrP coating immersed in D-Hank's solution.

FIGURE 8 | Cell proliferation in extracts after 1, 3 and 5 days of incubation measured by CCK-8 assay. Statistically (n 3 (**) indicate, $p < 0.01$ while (***) indicate $p < 0.03$).

immersion on the first day, much lower than that of Mg coating on the first day, after that, its downward pH trend is much slower than that of Mg coating, showing more Mg coating left in the Mg/SrP coating and presenting higher pH values in a more extended degradation period.

The deposition of SrP coating protected the Mg coating from degradation, but the existence of small non-uniform pores permeated the solution to inert the inner layer, and the degradation of Mg coating occurred. When Mg^{2+} ions dissolved into the solution, the cation reacted with OH^- to

TABLE 3 | Fitting results of Mg and Mg/SrP coatings immersed in D-Hank's solution.

Samples	R$_1$ (ohm)	Y04 (S * s^n)	C (F)	R$_2$ (ohm)
Mg coating	22.23	2.963×10^{-4}	0.543	7,160
Mg/SrP coating	18.34	2.123×10^{-4}	0.632	7,533

form $Mg(OH)_2$ in the solution. There is a release of Mg^{2+} ions during a different period, with both Mg coated and Mg/SrP coated samples indicating a rising tendency. After 7 days of immersion, the numbers of ions gradually rise to 73 and 69 ppm respectively, which is an indication of the continuous degradation of Mg coating.

Although Mg coating has well-established biocompatibility, its uncontrolled degradation and corrosion in the body fluid are the main factors affecting its reliability to support bone growth or tissues healing process. Also, the degradation of Mg causes hydrogen evolution (Witte et al., 2008). Both the formation of hydrogen gas cavities and the alkalization of the body fluid around the tissues interfere with the adhesion of the cell to
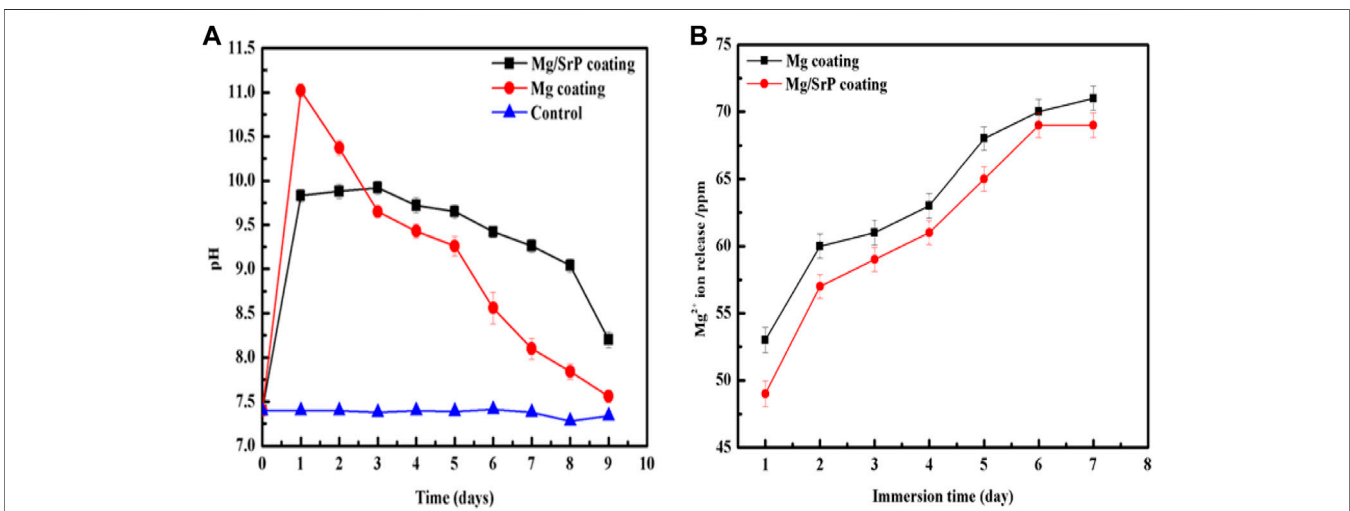

FIGURE 7 | pH change **(A)** and Mg^{2+} ions release **(B)** of the coatings at different immersion time in D-Hank's solution.

the implants. The presence of SrP coating on pure Mg coated implants reduced these phenomena. The release of Mg^{2+} ions around the implant overlaps the osteoblastic lineage and cell proliferation, which leads to the regeneration of bone tissues.

Cell Proliferation

Mg-Sr alloy containing a trace element of strontium may stimulate and increase the formation of new bone (Gu et al., 2012; Tie et al., 2016).

Figure 7 shows the cell proliferation assessment during the first 5 days. At 1st day, Mg/SrP coating cultured with cells showed relatively comparable absorbance, while Mg coating had a relatively lower absorbance in comparison with the control group. However, the absorbance, after 3 days, increased drastically for the entire group. At Day 3 and 5, Mg/SrP showed a relative increase in cell proliferation as compared to Mg coating and Ti groups. At day one, it is revealed from **Figure 8** that Mg coating shows a lower value of Optical Density (OD) as compared to the control, meaning that cell proliferation was inhibited because of the slight increase in pH value of the medium (Yang et al., 2013) which is not suitable for murine BMSCs to be adapted in the early stage. But cytoplasmic membrane would not disrupt due to the variation of pH. It's because the human body fluid is a considerable buffer system, which can very well adjust the pH of the physiological system. After 3 and 5 days, the absorbance measurements increased drastically for all groups, and no noticeable change was found. The results of 5 days demonstrate no cytotoxicity effect for both Mg and Mg/SrP coated implants. Furthermore, the overall proliferation of Mg/SrP group is better than the other group, due to the controlled release of ions and slower degradation of the coating. Mg^{2+} and Sr^{2+} ions in the coating surface have been found to accelerate diffusion, cell adhesion which favor effect on the mineralization and to improve cell proliferation (Cao et al., 2019).

CONCLUSION

In the present work, Mg/SrP composite coating was prepared on Ti6Al4V alloy. Mg/SrP coating initiated from the formation of $MgO/Mg(OH)_2$ carrying SrP: After immersion in the solution containing ammonium dihydrogen phosphate and strontium, the conversion reaction developed, $MgO/Mg(OH)_2$–SrP flakes into duplex coating, which cover the entire Mg coating after 10 min. Such coating system reduced the degradation rate of pure Mg coating and will serve in the future to control the degradation of Mg base coating. Further Mg/SrP coating cultured extract show high proliferation of MC3T3-E1 cells compared with normal culture medium. These results revealed that the Mg/SrP composite coating showed a higher corrosion resistance and exhibited significant biocompatibility compared with pure Mg coating on Ti alloy.

DATA AVAILABILITY STATEMENT

The raw data supporting the conclusions of this article will be made available by the authors, without undue reservation.

AUTHOR CONTRIBUTIONS

MI and XY performed the experiments and wrote the manuscript. KY and LT revised it.

FUNDING

REFERENCES

Attarilar, S., Salehi, M. T., Al-Fadhalah, K. J., Djavanroodi, F., and Mozafari, M. (2019). Functionally graded titanium implants: characteristic enhancement induced by combined severe plastic deformation. *PLoS One.* 14 (8), e0221491. doi:10.1371/journal.pone.0221491

Attarilar, S., Yang, J., Ebrahimi, M., Wang, Q., Liu, J., Tang, Y., et al. (2020). The toxicity phenomenon and the related occurrence in metal and metal oxide nanoparticles: a brief review from the biomedical perspective. *Front. Bioeng. Biotechnol.* 8, 822. doi:10.3389/fbioe.2020.00822

Boyd, A. R., Rutledge, L., Randolph, L., Mutreja, I., and Meenan, B. J. (2015). The deposition of strontium-substituted hydroxyapatite coatings. *J. Mater. Sci. Mater. Med.* 26 (2), 65. doi:10.1007/s10856-014-5377-z

Cao, L., Ullah, I., Li, N., Niu, S., Sun, R., Xia, D., et al. (2019). Plasma spray of biofunctional (Mg, Sr)-substituted hydroxyapatite coatings for titanium alloy implants. *J. Mater. Sci. Technol.* 35 (5), 719–726. doi:10.1016/j.jmst.2018.10.020

Chai, H., Guo, L., Wang, X., Gao, X., Liu, K., Fu, Y., et al. (2012). *In vitro* and *in vivo* evaluations on osteogenesis and biodegradability of a β-tricalcium phosphate coated magnesium alloy. *J. Biomed. Mater. Res.* 100A (2), 293–304. doi:10.1002/jbm.a.33267

Chen, J., Zhang, Y., Ibrahim, M., Etim, I. P., Tan, L., and Yang, K. (2019). *In vitro* degradation and antibacterial property of a copper-containing micro-arc oxidation coating on Mg-2Zn-1Gd-0.5Zr alloy. *Colloids Surf. B Biointerfaces.* 179, 77–86. doi:10.1016/j.colsurfb.2019.03.023

Drago, C., and Howell, K. (2012). Concepts for designing and fabricating metal implant frameworks for hybrid implant prostheses. *J. Prosthodont.* 21 (5), 413–424. doi:10.1111/j.1532-849x.2012.00835.x

Ebrahimi, M., Attarilar, S., Shaeri, M. H., Gode, C., Armoon, H., and Djavanroodi, F. (2019). An investigation into the effect of alloying elements on corrosion behavior of severely deformed Cu-Sn alloys by equal channel angular pressing. *Arch. Civ. Mech. Eng.* 19, 842–850. doi:10.1016/j.acme.2019.03.009

Gode, C., Attarilar, S., Eghbali, B., and Ebrahimi, M. (2015). "Electrochemical behavior of equal channel angular pressed titanium for biomedical application," AIP Conference Proceeding. 020041, 1-9. doi:10.1063/1.4914232.

Gu, X., Xie, X., Li, N., Zheng, Y., and Qin, L. (2012). *In vitro* and *in vivo* studies on a Mg-Sr binary alloy system developed as a new kind of biodegradable metal. *Acta Biomaterialia.* 8 (6), 2360–2374. doi:10.1016/j.actbio.2012.02.018

Hafeez, N., Liu, J., Wang, L., Wei, D., Tang, Y., Lu, W., et al. (2020). Superelastic response of low-modulus porous beta-type Ti-35Nb-2Ta-3Zr alloy fabricated by laser powder bed fusion. *Addit. Manuf.* 34, 101264. doi:10.1016/j.addma.2020.101264

Ibrahim, M., Yu, X., Chen, J., Etim, I. P., Misra, R. D. K., Tan, L., et al. (2020). Fabrication of biodegradable MgXCu(X=0, 0.1, 0.4, 0.7) coating on Ti6Al4V alloy with enhanced antibacterial property. *Mater. Technol.*, 1–10. doi:10.1080/10667857.2020.1738672

Ke, C., Pohl, K., Birbilis, N., and Chen, X.-B. (2014). Protective strontium phosphate coatings for magnesium biomaterials. *Mater. Sci. Technol.* 30 (5), 521–526. doi:10.1179/1743284714y.0000000508

Kraus, T., Fischerauer, S. F., Hänzi, A. C., Uggowitzer, P. J., Löffler, J. F., and Weinberg, A. M. (2012). Magnesium alloys for temporary implants in osteosynthesis: in vivo studies of their degradation and interaction with bone. *Acta Biomater.* 8 (3), 1230–1238. doi:10.1016/j.actbio.2011.11.008

Le, V. Q., Pourroy, G., Cochis, A., Rimondini, L., Abdel-Fattah, W. I., Mohammed, H. I., et al. (2014). Alternative technique for calcium phosphate coating on titanium alloy implants, *Biomatter* 4 (1), e28534. doi:10.4161/biom.28534

Li, H., Zheng, Y., and Qin, L. (2014a). Progress of biodegradable metals. *Prog. Nat. Sci.: Materials International.* 24 (5), 414–422. doi:10.1016/j.pnsc.2014.08.014

Li, R. W., Kirkland, N. T., Truong, J., Wang, J., Smith, P. N., Birbilis, N., et al. (2014b). The influence of biodegradable magnesium alloys on the osteogenic differentiation of human mesenchymal stem cells. *J. Biomed. Mater. Res.* 102 (12), 4346–4357. doi:10.1002/jbm.a.35111

Li, X. K., Gao, P., Wan, P., Pei, Y. F., Shi, L., Fan, B., et al. (2017). Novel bio-functional magnesium coating on porous Ti6Al4V orthopaedic implants: in vitro and in vivo study. *Sci. Rep.* 7, 40755. doi:10.1038/srep40755

Liu, S., Liu, J., Wang, L., Ma, R. L.-W., Zhong, Y., Lu, W., et al. (2020). Superelastic behavior of *in-situ* eutectic-reaction manufactured high strength 3D porous NiTi-Nb scaffold. *Scripta Mater.* 181, 121–126. doi:10.1016/j.scriptamat.2020.02.025

Liu, X., Chu, P., and Ding, C. (2004). Surface modification of titanium, titanium alloys, and related materials for biomedical applications. *Mater. Sci. Eng. R Rep.* 47 (3), 49–121. doi:10.1016/j.mser.2004.11.001

Salunke, P., Shanov, V., and Witte, F. (2011). High purity biodegradable magnesium coating for implant application. *Mater. Sci. Eng., B* 176 (20), 1711–1717. doi:10.1016/j.mseb.2011.07.002

Staiger, M. P., Pietak, A. M., Huadmai, J., and Dias, G. (2006). Magnesium and its alloys as orthopedic biomaterials: a review. *Biomaterials* 27 (9), 1728–1734. doi:10.1016/j.biomaterials.2005.10.003

Sun, Y., Zhang, B., Wang, Y., Geng, L., and Jiao, X. (2012). Preparation and characterization of a new biomedical Mg-Zn-Ca alloy. *Mater. Des.* 34, 58–64. doi:10.1016/j.matdes.2011.07.058

Tie, D., Guan, R., Liu, H., Cipriano, A., Liu, Y., Wang, Q., et al. (2016). An in vivo study on the metabolism and osteogenic activity of bioabsorbable Mg-1Sr alloy. *Acta Biomater.* 29, 455–467. doi:10.1016/j.actbio.2015.11.014

Wang, J., Witte, F., Xi, T., Zheng, Y., Yang, K., Yang, Y., et al. (2015). Recommendation for modifying current cytotoxicity testing standards for biodegradable magnesium-based materials. *Acta Biomater.* 21, 237–249. doi:10.1016/j.actbio.2015.04.011

Wang, Q., Zhou, P., Liu, S., Attarilar, S., Ma, R. L.-W., Zhong, Y., et al. (2020). Multi-scale surface treatments of titanium implants for rapid osseointegration: a review. *Nanomaterials* 10 (6), 1244. doi:10.3390/nano10061244

Witte, F. (2015). Reprint of: the history of biodegradable magnesium implants: a review. *Acta Biomater.* 23, S28–S40. doi:10.1016/j.actbio.2015.07.017

Witte, F., Fischer, J., Nellesen, J., Crostack, H.-A., Kaese, V., Pisch, A., et al. (2006). *In vitro* and *in vivo* corrosion measurements of magnesium alloys. *Biomaterials* 27 (7), 1013–1018. doi:10.1016/j.biomaterials.2005.07.037

Witte, F., Hort, N., Vogt, C., Cohen, S., Kainer, K. U., Willumeit, R., et al. (2008). Degradable biomaterials based on magnesium corrosion. *Curr. Opin. Solid State Mater. Sci.* 12 (5-6), 63–72. doi:10.1016/j.cossms.2009.04.001

Witte, F., Kaese, V., Haferkamp, H., Switzer, E., Meyer-Lindenberg, A., Wirth, C., et al. (2005). *In vivo* corrosion of four magnesium alloys and the associated bone response. *Biomaterials* 26 (17), 3557–3563. doi:10.1016/j.biomaterials.2004.09.049

Yang, X., Li, M., Lin, X., Tan, L., Lan, G., Li, L., et al. (2013). Enhanced *in vitro* biocompatibility/bioactivity of biodegradable Mg-Zn-Zr alloy by micro-arc oxidation coating contained Mg_2SiO_4. *Surf. Coating. Technol.* 233, 65–73. doi:10.1016/j.surfcoat.2013.01.052

Yu, X., Ibrahim, M., Liu, Z., Yang, H., Tan, L., and Yang, K. (2018a). Biofunctional Mg coating on PEEK for improving bioactivity. *Bioact. Mater.* 3 (2), 139–143. doi:10.1016/j.bioactmat.2018.01.007

Yu, X., Ibrahim, M., Lu, S., Yang, H., Tan, L., and Yang, K. (2018b). MgCu coating on Ti6Al4V alloy for orthopedic application. *Mater. Lett.* 233, 35–38. doi:10.1016/j.matlet.2018.08.063

Zhai, Z., Qu, X., Li, H., Yang, K., Wan, P., Tan, L., et al. (2014). The effect of metallic magnesium degradation products on osteoclast-induced osteolysis and attenuation of NF-κB and NFATc1 signaling. *Biomaterials* 35 (24), 6299–6310. doi:10.1016/j.biomaterials.2014.04.044

Zhang, L. C., and Chen, L. Y. (2019). A review on biomedical titanium alloys: recent progress and prospect. *Adv. Eng. Mater.* 21 (4), 1801215. doi:10.1002/adem.201801215

Zheng, Y. F., Gu, X. N., and Witte, F. (2014). Biodegradable metals. *Mater. Sci. Eng. R Rep.* 77, 1–34. doi:10.1016/j.mser.2014.01.001